



RESEARCH MEMORANDUM

EFFECT OF LARGE NEGATIVE DIHEDRAL OF THE HORIZONTAL TAIL
ON LONGITUDINAL AND LATERAL STABILITY CHARACTERISTICS
OF A SWEPT-WING CONFIGURATION AT
TRANSONIC SPEEDS

By Donald D. Arabian

Langley Aeronautical Laboratory
Langley Field, Va.

NATIONAL ADVISORY COMMITTEE
FOR AERONAUTICS
WASHINGTON

January 17, 1956
Declassified September 17, 1958

NATIONAL ADVISORY COMMITTEE FOR AERONAUTICS

RESEARCH MEMORANDUM

EFFECT OF LARGE NEGATIVE DIHEDRAL OF THE HORIZONTAL TAIL

ON LONGITUDINAL AND LATERAL STABILITY CHARACTERISTICS

OF A SWEPT-WING CONFIGURATION AT

TRANSONIC SPEEDS

By Donald D. Arabian

SUMMARY

The longitudinal and lateral stability characteristics of a 40° swept-wing fighter model with and without horizontal tails of 0° and $22\frac{1}{2}^{\circ}$ negative dihedral are presented for Mach numbers from 0.80 to 1.05 for a range of angles of attack and sideslip.

The results of the investigation indicate that the horizontal tail with negative dihedral reduced the lift-coefficient and pitching-moment range over which longitudinal instability existed for the model equipped with a horizontal tail without dihedral. In addition, the stability contribution of the horizontal tail with negative dihedral to the overall longitudinal stability of the model was stabilizing for all test conditions, whereas that of the horizontal tail without dihedral was destabilizing at the high lift coefficients.

The horizontal tail with negative dihedral increased the directional-stability parameter $C_{n\beta}$ and slightly decreased the effective dihedral parameter $C_{l\beta}$.

INTRODUCTION

The longitudinal instability that occurs for some swept-wing airplanes operating at high lift coefficients has been found to result from flow separation on the wing or improper location of the horizontal tail or a combination of both conditions. Consequently, the use of various wing fixes has been studied in an attempt to alleviate wing-flow separation. The results of some of these studies are summarized in reference 1. Studies of horizontal-tail location, such as references 1

and 2, have shown that the longitudinal stability of a model can be altered by the vertical location of the horizontal tail because of the variation of the downwash throughout the flow field behind the wing.

The analysis in reference 2 of the flow in the vicinity of the horizontal-tail location behind a sweptback wing indicated that at high angles of attack the variation of downwash with angle of attack over the outer sections of the tail span was such that the tail contribution to the longitudinal stability was favorable for the position below the extended wing-chord plane and destabilizing for the positions above the extended wing-chord plane. It should be possible therefore, in cases where a low tail location is impractical, to incorporate some of the advantages of a low tail by mounting the tail in a higher position and incorporating negative dihedral.

During a recent low-speed investigation in the Langley 19-foot pressure tunnel, of a swept-wing fighter model equipped with wing fences and a modified leading edge outboard of the fences, it was found that longitudinal instability occurred at high lift coefficients. Various horizontal-tail arrangements were tried to improve the stability. One arrangement consisted of setting the horizontal tail with 22° of negative dihedral which gave some improvement in stability in the high lift range.

However, it was of interest to determine the effects of a horizontal tail with negative dihedral on the stability characteristics of the model at transonic speeds. Therefore, a study was made of a similar swept-wing fighter airplane model with wing fixes in the Langley 16-foot transonic tunnel to determine the effect on the longitudinal and lateral stability

characteristics of a 40° swept horizontal tail set with $22\frac{1}{2}^{\circ}$ of negative dihedral. The data for the model without a horizontal tail, with a straight horizontal tail, and with a negative-dihedral horizontal tail are presented in this paper for a Mach number range from 0.80 to 1.05 and for a range of angles of attack and of sideslip.

SYMBOLS

All moments are taken about the stability axis originating in the plane of symmetry at $0.21\bar{c}$ (see fig. 1).

b wing span, ft

C_D drag coefficient, $\frac{\text{Drag}}{qS_w}$

C_{D_i} internal drag coefficient, $\frac{\text{Internal drag}}{qS_w}$

C_L lift coefficient, $\frac{\text{Lift}}{qS_w}$

C_l rolling-moment coefficient, $\frac{\text{Rolling moment}}{qS_w b}$

C_m pitching-moment coefficient, $\frac{\text{Pitching moment}}{qS_w \bar{c}_w}$

C_n yawing-moment coefficient, $\frac{\text{Yawing moment}}{qS_w b}$

C_Y lateral-force coefficient, $\frac{\text{Lateral force}}{qS_w}$

$$C_{l\beta} = \frac{\partial C_l}{\partial \beta} \text{ per deg}$$

$$C_{n\beta} = \frac{\partial C_n}{\partial \beta} \text{ per deg}$$

$$C_{Y\beta} = \frac{\partial C_Y}{\partial \beta} \text{ per deg}$$

c local chord, ft

\bar{c} mean aerodynamic chord, $\frac{2}{S} \int_0^{b/2} c^2 dy$, ft

l tail length of $0.21\bar{c}$ of wing to $0.25\bar{c}$ of horizontal tail

M Mach number

m/m_∞ mass-flow ratio, $\frac{\text{Actual mass flow}}{\text{Ideal mass flow}}$

S area, sq ft

q free-stream dynamic pressure, lb/sq ft

y spanwise distance from plane of symmetry, ft

α angle of attack measured from fuselage reference, deg

β sideslip angle, deg

τ horizontal-tail stability parameter,

$$\frac{1}{\frac{S_t l}{S_w c_w} \left(\frac{dc_{L_t}}{da_t} \right)} \left(\frac{dc_{m_t}}{da} \right)$$

isolated

Subscripts:

t horizontal tail

w wing

MODEL AND TESTS

Model

The general arrangement of the swept-wing fighter model is shown in figure 2. Two horizontal tails with different dihedral angles were investigated. For the sake of convenience, the tail having 0° of dihedral will hereinafter be referred to as the plane tail, whereas the one with

$-22\frac{1}{2}^\circ$ of dihedral will be referred to as the drooped tail. For the tests of the model with the drooped tail, the plane tail was replaced by one which had each panel of the plane tail rotated down about the root section through $22\frac{1}{2}^\circ$ (dashed in fig. 2(a)). This effectively decreased the projected span of the horizontal tail.

The root chord line of both the plane and drooped tails was located vertically 5.3 inches above the fuselage reference line and had NACA 64A009 constant chord sections normal to the 40° swept leading edge.

The geometry of the wing was as follows: aspect ratio, 3.43; taper ratio, 0.578; quarter-chord-line sweep, 40° ; and airfoil section normal to the quarter chord, NACA 64A010. The incidence of the wing was 1.5° with respect to the fuselage reference line.

The wing included modifications to improve the flow characteristics. (See fig. 2(b).) Two fences were located on each wing panel and extended around the leading edge to the lower surface. The leading-edge modification which extended from the outermost fence, $0.675b/2$, to the tip of the wing was characterized by a doubling of the leading-edge radius. The center of the increased leading-edge radius was located so that the camber was effectively increased.

The wing inlets were ducted to expel air around the sting through the tail pipe.

Photographs of the model mounted on the sting in the tunnel are shown in figure 3.

Tests

The tests were conducted in the Langley 16-foot transonic tunnel which is described in reference 3. The Mach number range was from 0.80 to 1.05 which corresponded to a Reynolds number range from about 5.1×10^6 to 5.4×10^6 based on the wing mean aerodynamic chord. The angles of attack and sideslip at which each configuration was tested were as follows:

| Configuration | α , deg | β , deg |
|-------------------------------|---------------------------------------|-------------------------|
| Model with plane tail | -2 to 16 -2 to 16 -2 to 16 0 | 0 5 -5 -5 to 5 |
| Model with drooped tail | -2 to 16 -2 to 16 | 0 5 |
| Model without horizontal tail | -2 to 16 | 0 |

The horizontal tail was set at 0° incidence for all tests.

The forces and moments were measured by a six-component strain-gage balance mounted internally to the model and attached to the sting-support system which allows the angle of attack to be changed without appreciably changing the model location in the tunnel. A description of the sting-support system is given in reference 4.

DATA REDUCTION

All the drag data have been corrected by adjusting the base pressure to free-stream static pressure and by subtracting the internal drag. The internal drag was determined as suggested in reference 5. The mean stagnation pressure over the exit area was obtained by weighing eight individual total-pressure tubes according to the percentage of the total exit area that each tube represented and summing the results.

The mass-flow ratio m/m_0 presented in figure 4 against angle of attack for a Mach number of 0.98 remained at about 0.72 and was typical of the variations of the mass flow with angle of attack for all the Mach numbers tested. Typical internal drag data are presented in figure 5 against angle of attack for three representative Mach numbers.

RESULTS AND DISCUSSION

Longitudinal Stability Characteristics

The variation of lift coefficient with angle of attack for a range of Mach numbers is presented in figure 6 for the model with the plane tail, with the drooped tail, and for the model without a horizontal tail. The slope of the lift curves for each of the configurations decreased at about C_L of 0.6 for Mach numbers less than 1.00. For the supersonic Mach numbers, the lift-curve slope decreased at the higher values of lift coefficient. The lift-curve slope was reduced slightly by drooping the horizontal tail.

The variation of pitching-moment coefficient with lift coefficient is presented in figure 7. The pitching-moment curve for the plane tail was included on the pitching-moment plots of both the drooped tail and horizontal tail-off configurations for comparison. The lift coefficient at which the longitudinal instability of the complete model occurred remained about the same for both horizontal-tail configurations, but the unstable pitching moments occurred over a smaller range of C_L and C_m values for the drooped tail. The contribution of both the plane and the drooped tail to the stability of the model was essentially the same up to C_L values where instability commenced. This is better illustrated in figure 8 where the tail-stability parameter τ is plotted against lift coefficient for the Mach number range investigated. In the preparation of the data of figure 8 the dynamic-pressure ratio at the tail was assumed to be 1,

and $dC_L/d\alpha$ of the isolated horizontal tail was taken to be 0.06. All the quantities in the expression of τ were assumed constant for both horizontal tails, except $dC_{m_t}/d\alpha$ which was determined from the experimental data. The horizontal tail contributes to the stability of the model if the sign of τ is negative.

Figure 8 shows that at low Mach numbers the contribution of the plane tail to the overall stability of the model was destabilizing above C_L values of 0.7. At the higher Mach numbers the plane tail had a stabilizing effect to higher values of lift coefficient. Note that drooping

the tail resulted in stabilizing contributions to the overall stability throughout the range of test conditions investigated. Although the stabilizing contribution of the drooped tail was reasonably consistent with lift coefficient it was not possible to overcome completely the large destabilizing contribution of the wing.

The drag characteristics are shown in figure 9 for the three configurations tested and the variation of the drag coefficients with Mach number is shown in figure 10 for C_L values of 0 and 0.3. Although the data of figure 10 are presented for untrimmed lift coefficients, it is believed that the out-of-trim drag coefficients presented would not alter the conclusions drawn from the comparisons.

As indicated in figure 10, the drooped tail produced a slight increase in drag above that for the basic configuration for the entire Mach number range at zero lift and at a C_L value of 0.3, although the pressure recovery on the aft portion of the fuselage was increased as shown by unpublished pressure data. The drag increase may be the result of an additional interference effect between the drooped tail and the vertical tail which could cause separation in the region of the intersection of the tail surfaces.

Lateral Stability Characteristics

The variation of the force and moment coefficients C_l , C_n , and C_y with sideslip and Mach number for 0° angle of attack is presented in figure 11 for the plane-tail configuration. Of significance is the change of the linear variation of C_l with β at the low Mach numbers to non-linear variations at the high Mach numbers. Positive dihedral effect occurred for the low Mach numbers, whereas negative dihedral effect was present for small sideslip angles for the higher Mach number range.

The derivatives $C_{l\beta}$, $C_{n\beta}$, and $C_{y\beta}$ were evaluated by taking the slope of the coefficient data between 0° and 5° of sideslip. The variation of the derivatives with lift coefficient for various Mach numbers is shown in figures 12(a), (b), and (c) for the model with the plane tail and for the model with the drooped tail. The derivative $C_{l\beta}$ remained negative for the low Mach numbers but became positive for the higher Mach numbers for C_L values less than 0.6. At the high C_L values, $C_{l\beta}$ tended to become negative for all Mach numbers. A comparison of $C_{l\beta}$ obtained for the two tail configurations indicated that the drooped tail decreased the values of $C_{l\beta}$ in general for values of C_L below those of which the

pitching moment becomes unstable. At higher lift coefficients, the effect of the drooped tail was inconsistent.

The variation of yawing moment with sideslip $C_{n\beta}$ remained stable up to the maximum lift coefficient. However, note that at the high C_L values the derivative $C_{n\beta}$ is rapidly approaching zero at the low Mach numbers. Essentially, $C_{n\beta}$ for the model with either horizontal tail was constant with C_L below the angle of attack at which the lift coefficient breaks. Negative dihedral on the horizontal tail effectively increased the vertical tail area and thus provided an increase of $C_{n\beta}$ throughout the Mach number and lift-coefficient range investigated.

The derivative $C_{Y\beta}$ which remained fairly constant with C_L , became more negative with the drooped tail.

CONCLUSIONS

The results of the longitudinal and lateral stability investigation of a swept-wing fighter model with a 0° dihedral horizontal tail and with a $22\frac{1}{2}^\circ$ negative dihedral tail indicated the following conclusions:

1. The horizontal tail with negative dihedral decreased the lift-coefficient and pitching-moment range over which longitudinal instability existed for the model with the horizontal tail without dihedral.
2. There was a stabilizing contribution from the horizontal tail with negative dihedral to the model stability for all test conditions, whereas destabilizing contributions existed for the horizontal tail without dihedral at the high lift coefficients.
3. A comparison of the lateral characteristics of the model between the two horizontal-tail configurations showed the horizontal tail with negative dihedral increased the directional-stability parameter $C_{n\beta}$.

and slightly decreased the effective dihedral parameter $C_{l\beta}$ for lift coefficients below those where the pitching moment becomes unstable.

Langley Aeronautical Laboratory,
National Advisory Committee for Aeronautics,
Langley Field, Va., Sept. 9, 1955.

REFERENCES

1. Furlong, G. Chester, and McHugh, James G.: A Summary and Analysis of the Low-Speed Longitudinal Characteristics of Swept Wings at High Reynolds Number. NACA RM L52D16, 1952.
2. Foster, Gerald V., and Griner, Roland F.: A Study of Several Factors Affecting the Stability Contributed by a Horizontal Tail at Various Vertical Positions on a Sweptback-Wing Airplane Model. NACA RM L9H19, 1949.
3. Ward, Vernon G., Whitcomb, Charles F., and Pearson, Merwin D.: Air-Flow and Power Characteristics of the Langley 16-Foot Transonic Tunnel With Slotted Test Section. NACA RM L52E01, 1952.
4. Hallissy, Joseph M., and Bowman, Donald R.: Transonic Characteristics of a 45° Sweptback Wing-Fuselage Combination. Effect of Longitudinal Wing Position and Division of Wing and Fuselage Forces and Moments. NACA RM L52K04, 1953.
5. Pendley, Robert E., Milillo, Joseph R., and Fleming, Frank F.: An Investigation of Three NACA 1-Series Nose Inlets at Subsonic and Transonic Speeds. NACA RM L52J23, 1953.

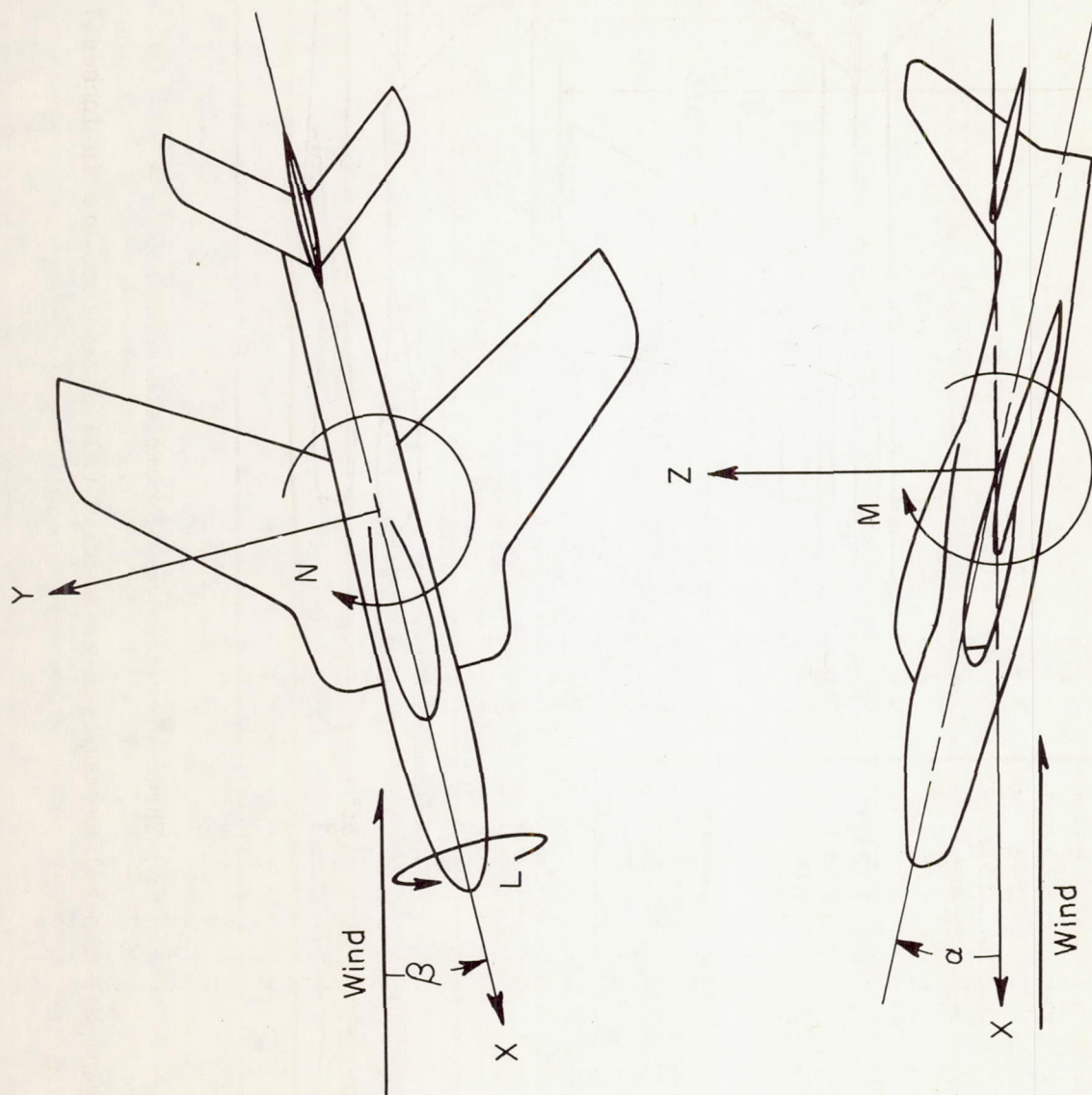


Figure 1.- Stability-axes system showing positive angles, forces, and moments.

MODEL GEOMETRY

Wing

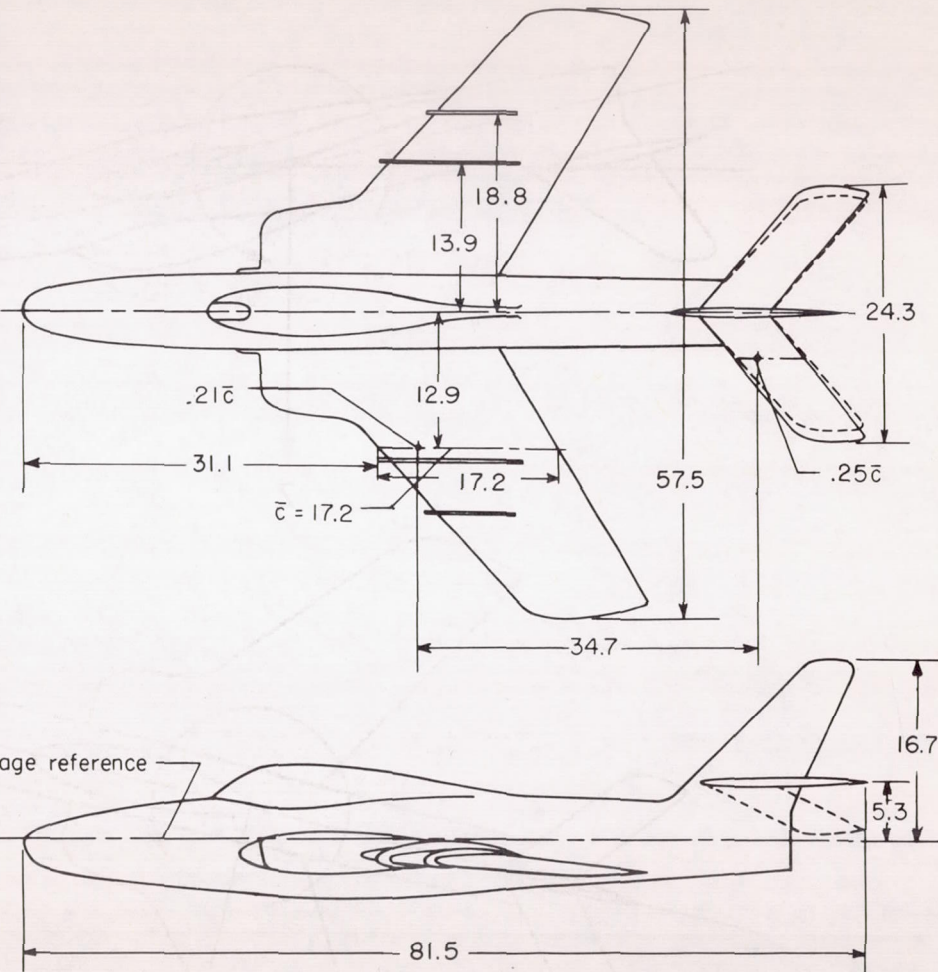
Airfoil section normal to C/4 NACA 64AO10
 Area excluding inlet extension 6.63 sq ft
 Aspect ratio 3.43
 Taper ratio 0.578
 Sweep at C/4 40°
 Incidence 1.5°

Horizontal tail

Area 1.13 sq ft
 Aspect ratio 3.59
 Taper ratio 1.0
 Sweep 40°

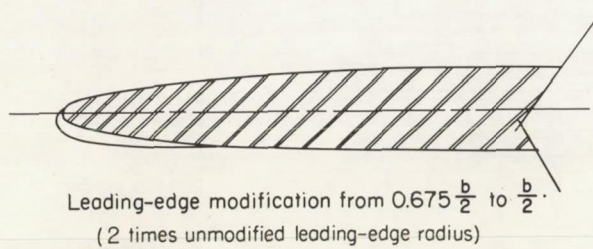
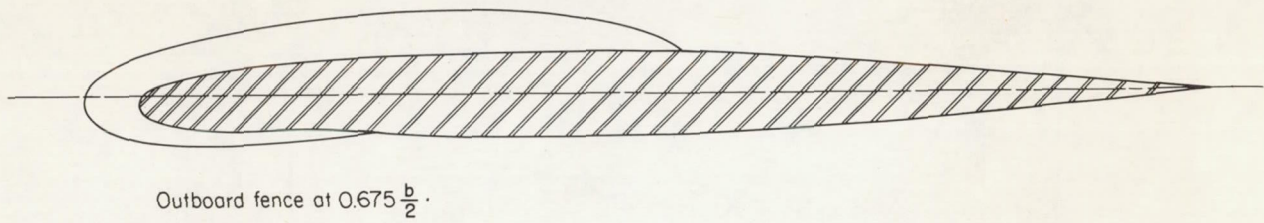
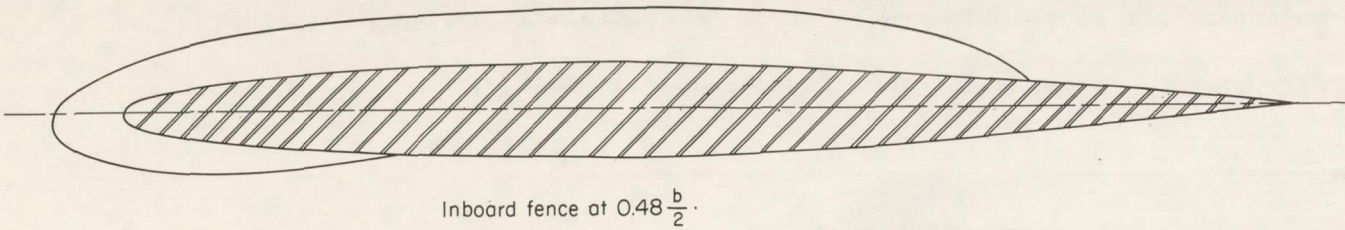
Vertical tail

Area 0.87 sq ft
 Aspect ratio 1.68
 Taper ratio 0.402
 Sweep C/4 41.27°



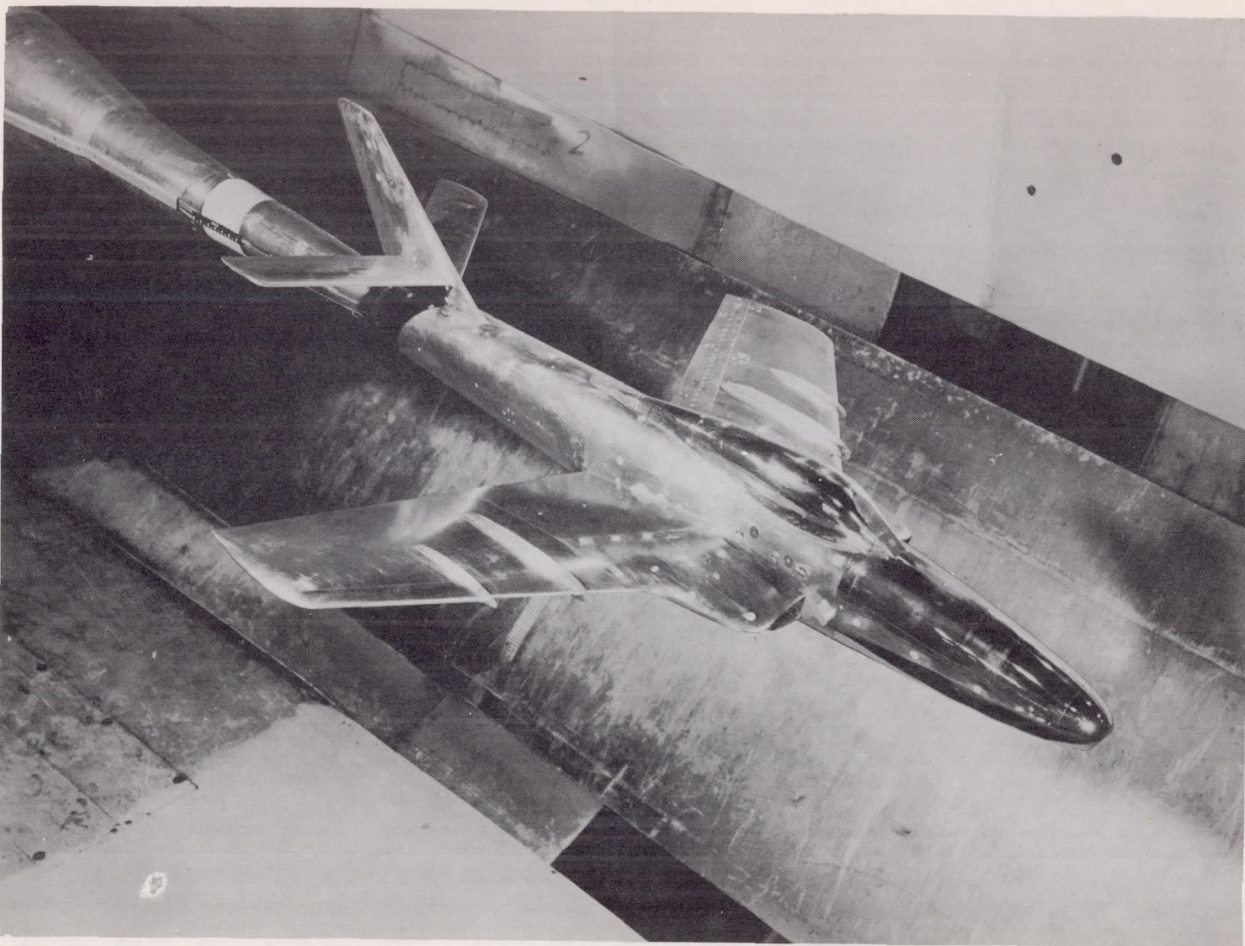
(a) Three-view drawing of complete model.

Figure 2.- General arrangement of model. (All dimensions are in inches.)



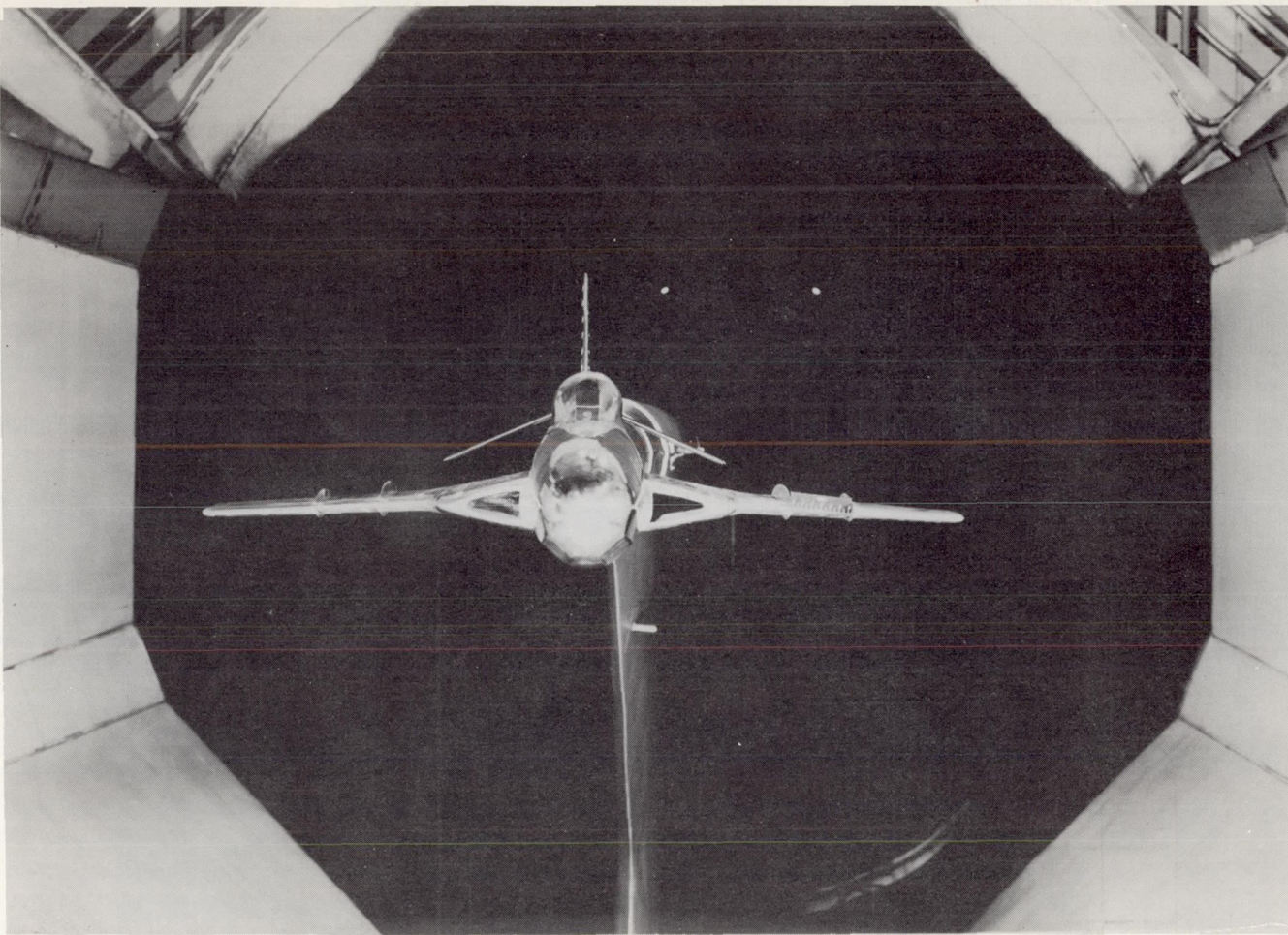
(b) Details of wing fixes and modifications.

Figure 2.- Concluded.



(a) Complete configuration with plane tail. L-85379

Figure 3.- Model mounted in Langley 16-foot transonic tunnel.



L-85400

(b) Yawed model with the drooped tail.

Figure 3.- Concluded.

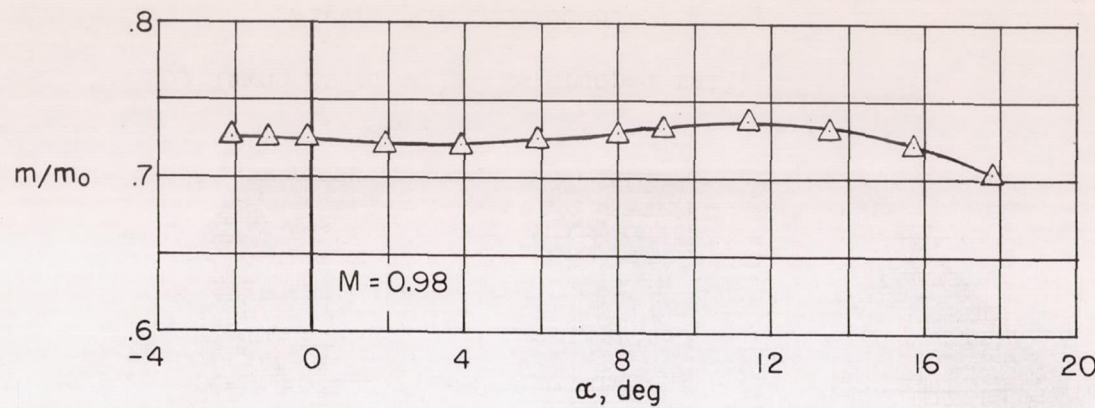


Figure 4.- Variation of mass-flow ratio with angle of attack.

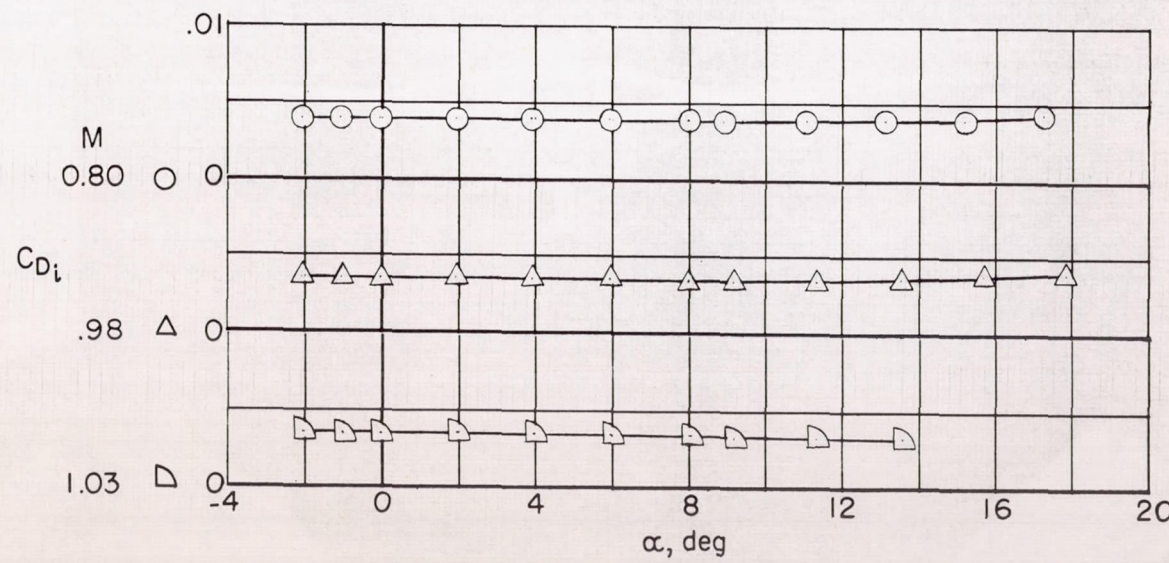
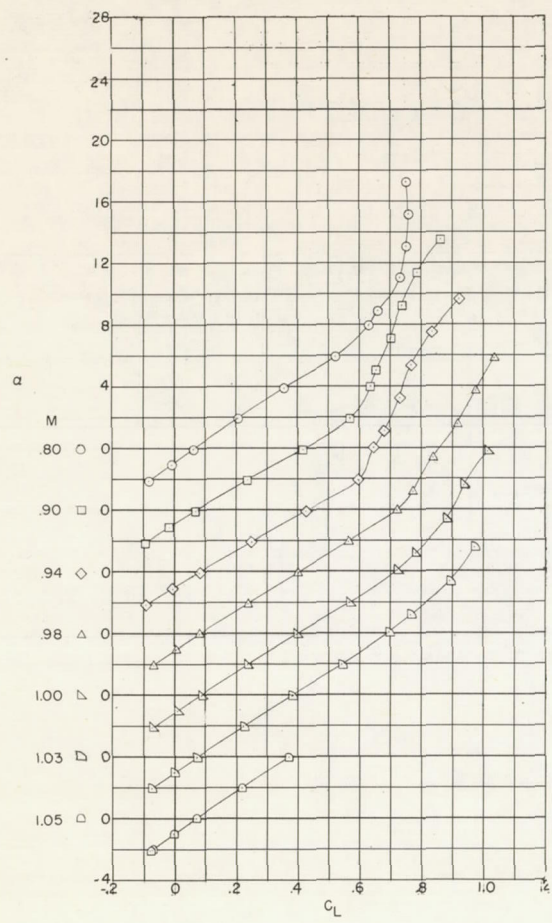
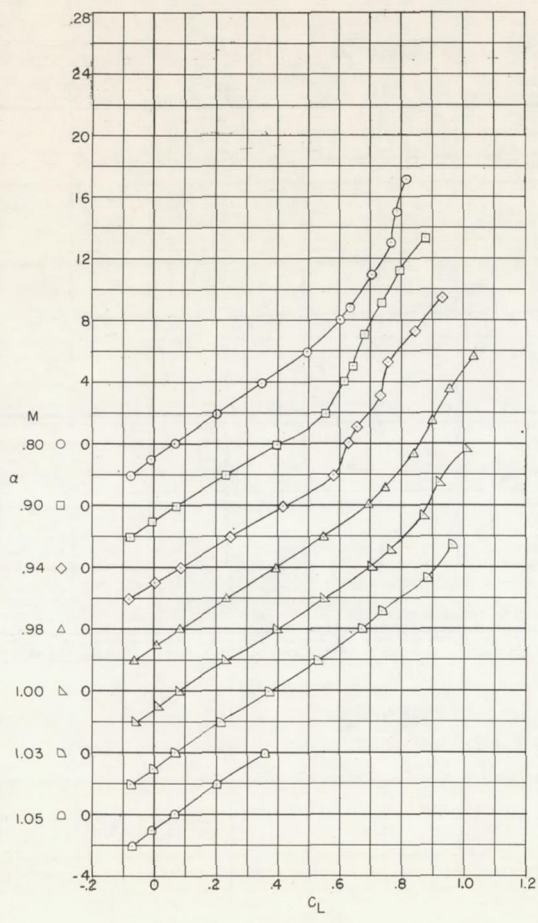


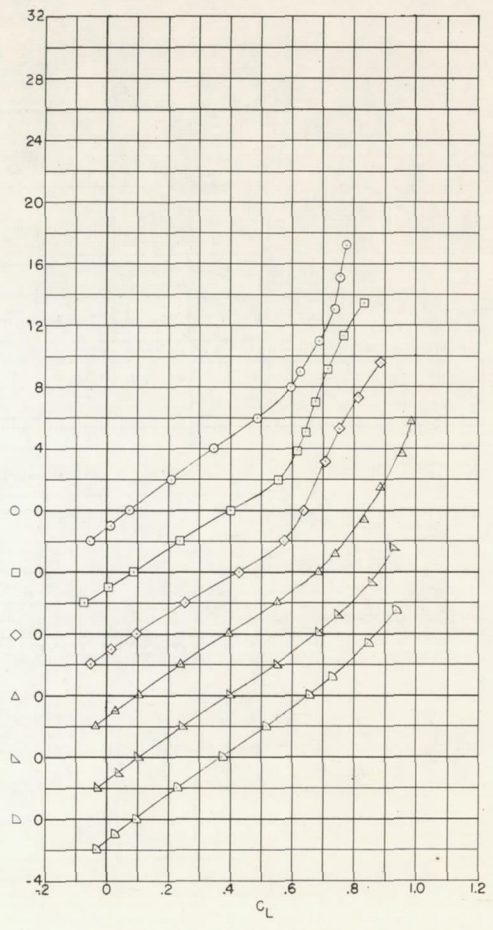
Figure 5.- Internal drag characteristics of complete model.



(a) Plane tail.

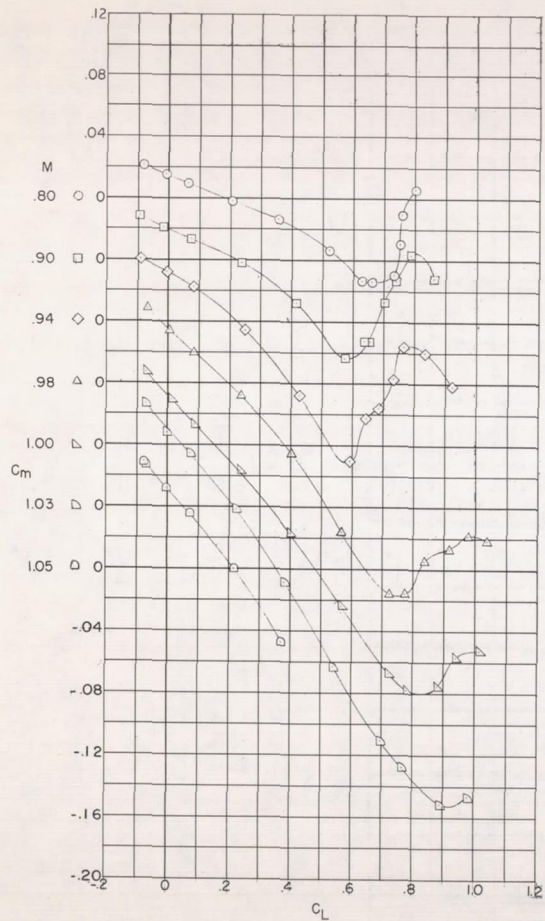


(b) Drooped tail.

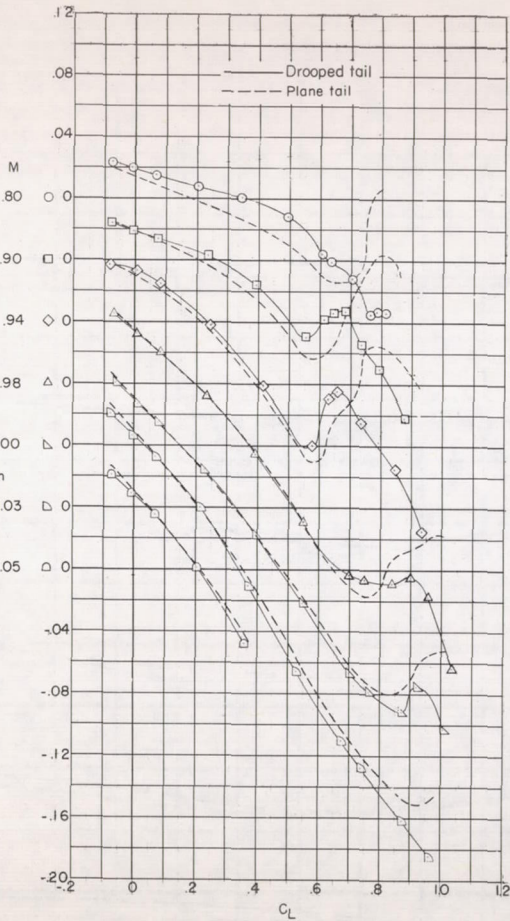


(c) Horizontal tail off.

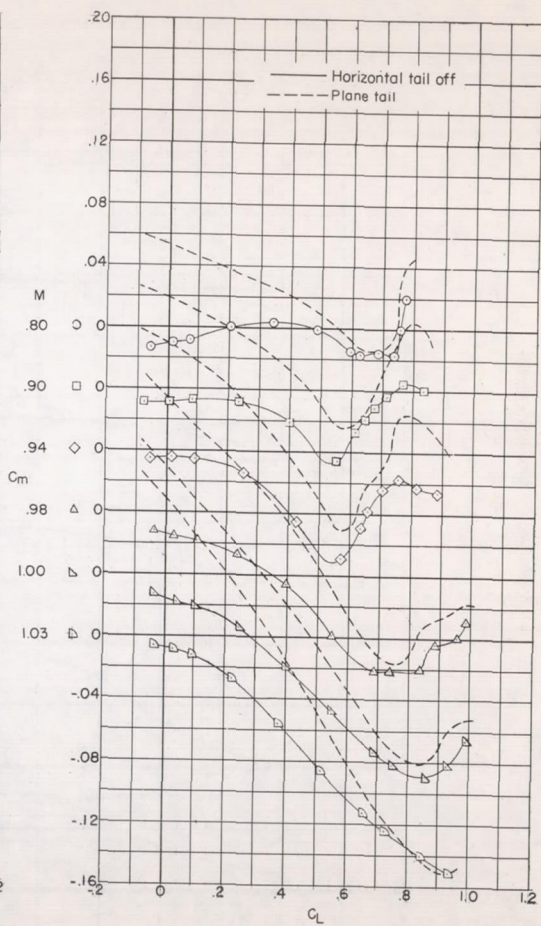
Figure 6.- Lift characteristics of model with various horizontal-tail configurations.



(a) Plane tail.



(b) Drooped tail.



(c) Horizontal tail off.

Figure 7.- Pitching-moment characteristics of model for various horizontal-tail configurations.

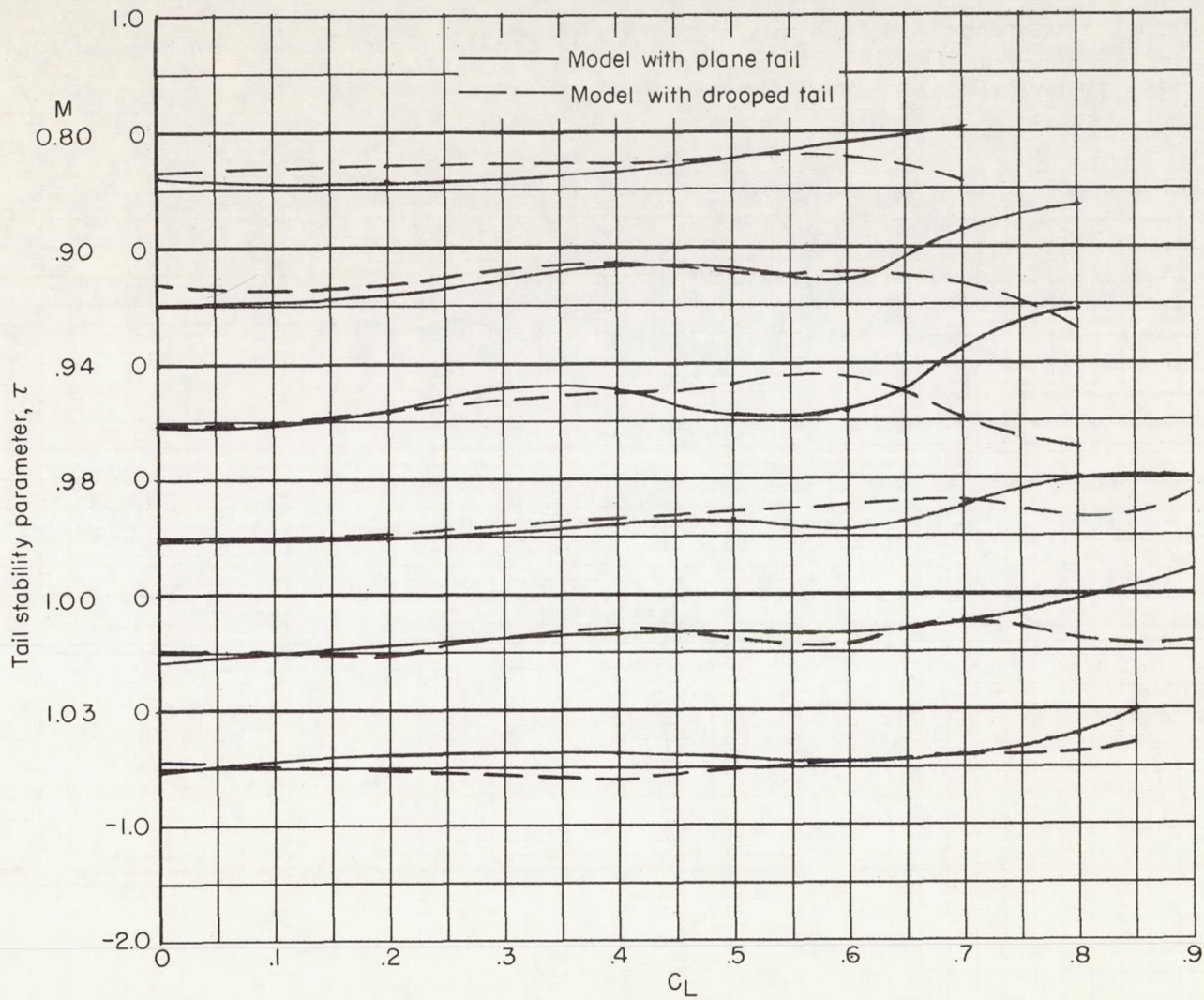
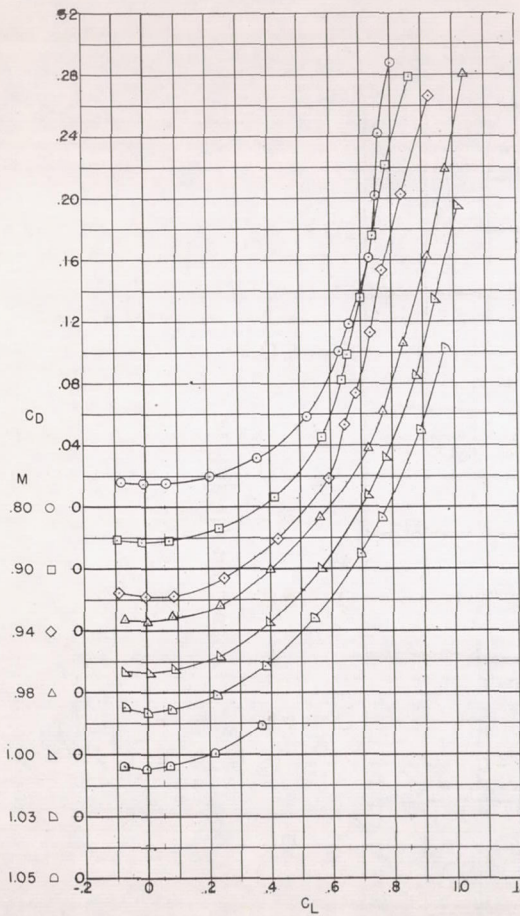
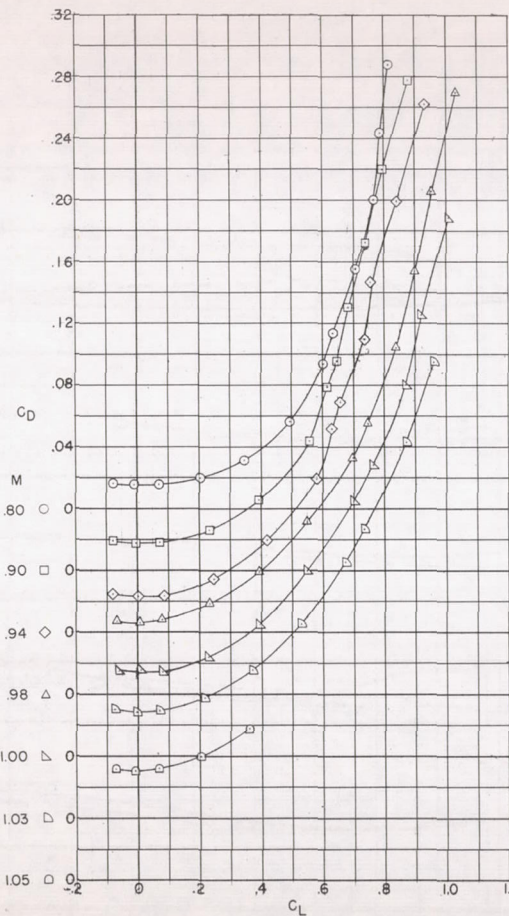


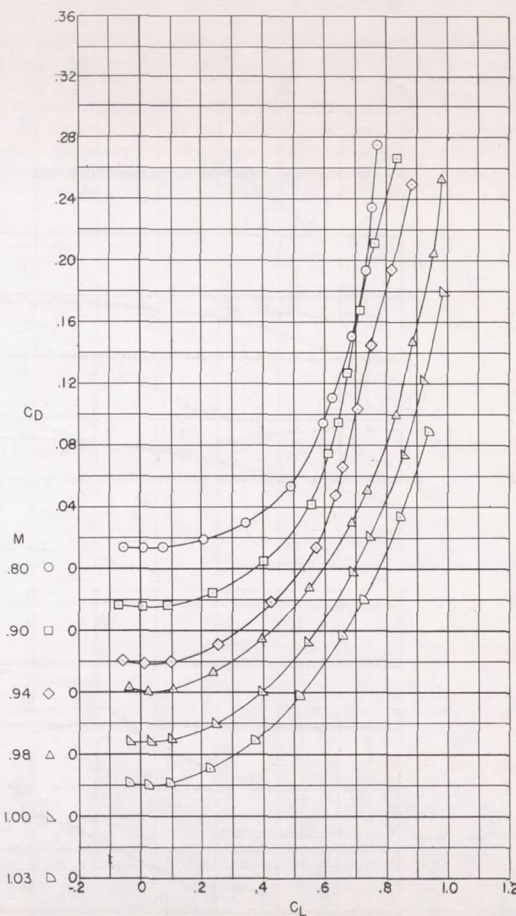
Figure 8.- Contribution of plane tail and drooped tail to stability.



(a) Plane tail.



(b) Drooped tail.



(c) Horizontal tail off.

Figure 9.- Drag characteristics of model for various horizontal-tail configurations.

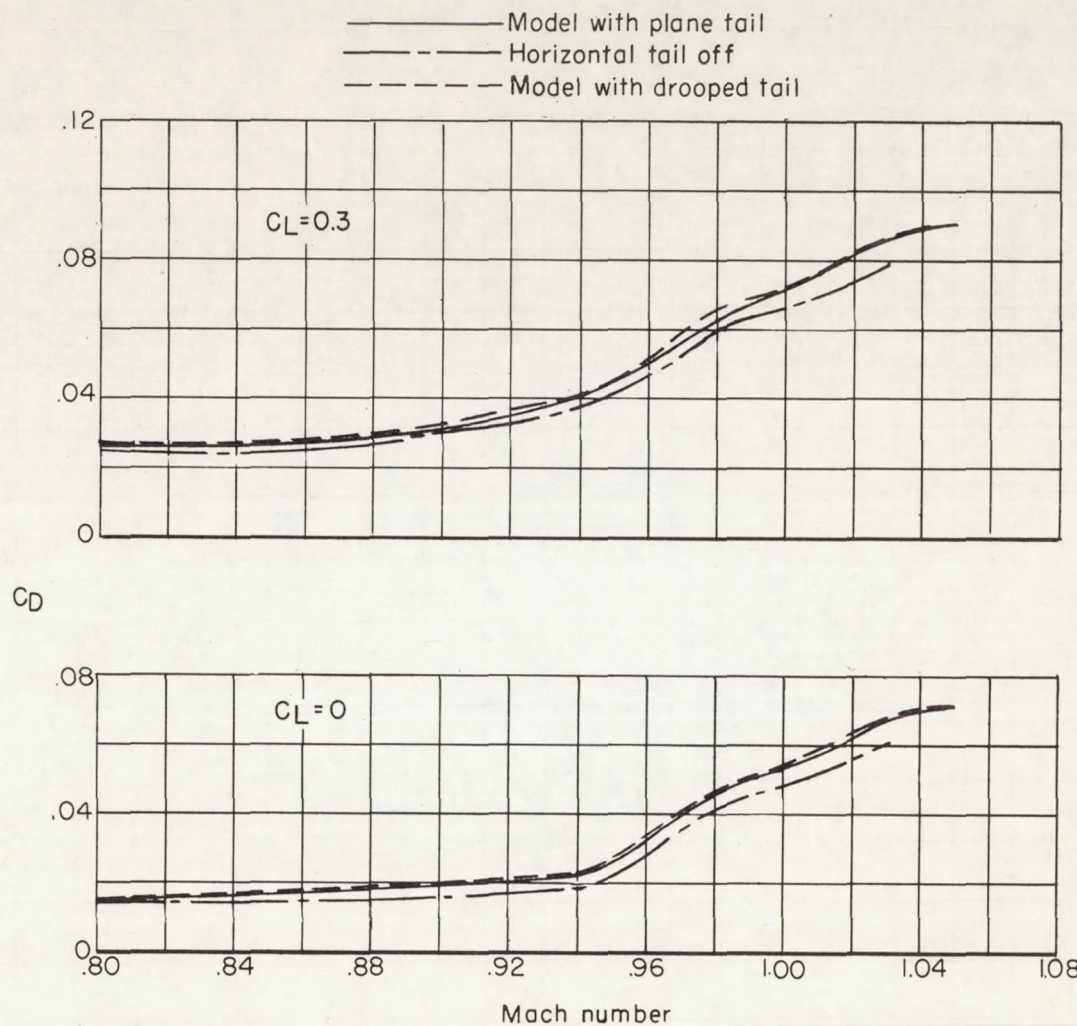


Figure 10.- Variation of drag coefficient with Mach number for configurations tested.
 $C_L = 0.3; C_L = 0.$

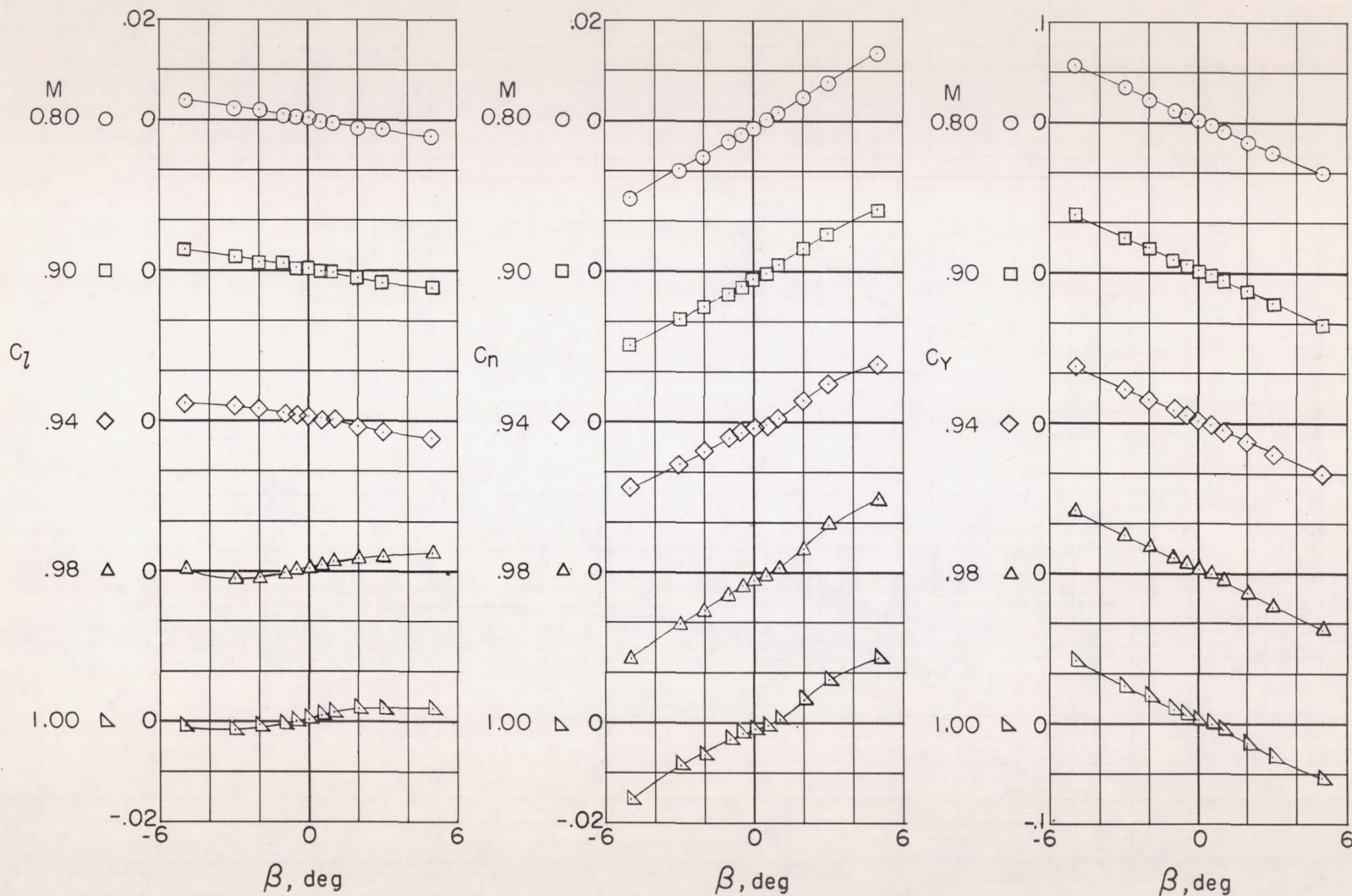


Figure 11.- Variation of static lateral force and moment coefficients with sideslip for model with plane tail. $\alpha = 0^\circ$.

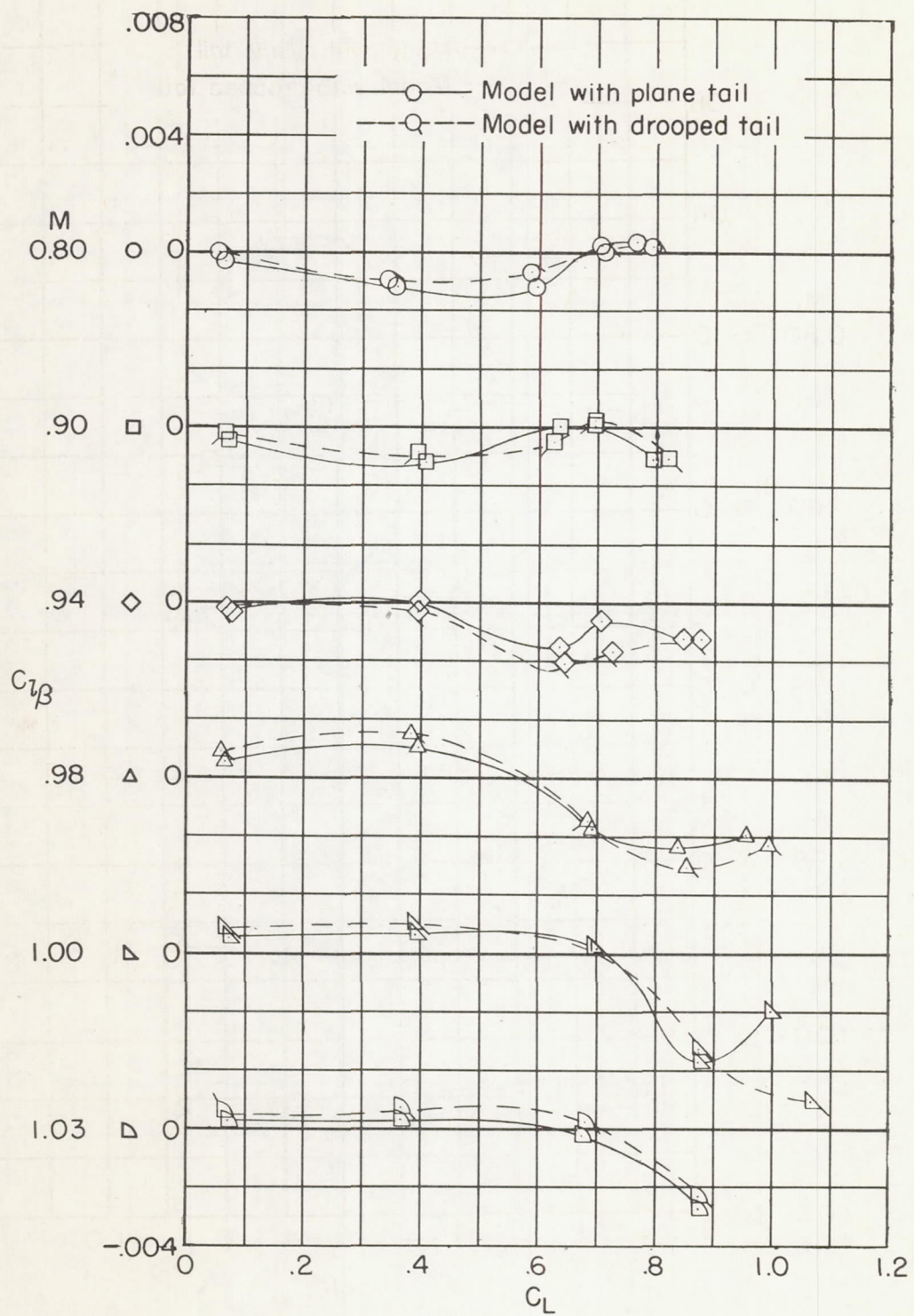
(a) $C_{l\beta}$ against C_L .

Figure 12.- Effect of drooped tail on static lateral stability derivatives.

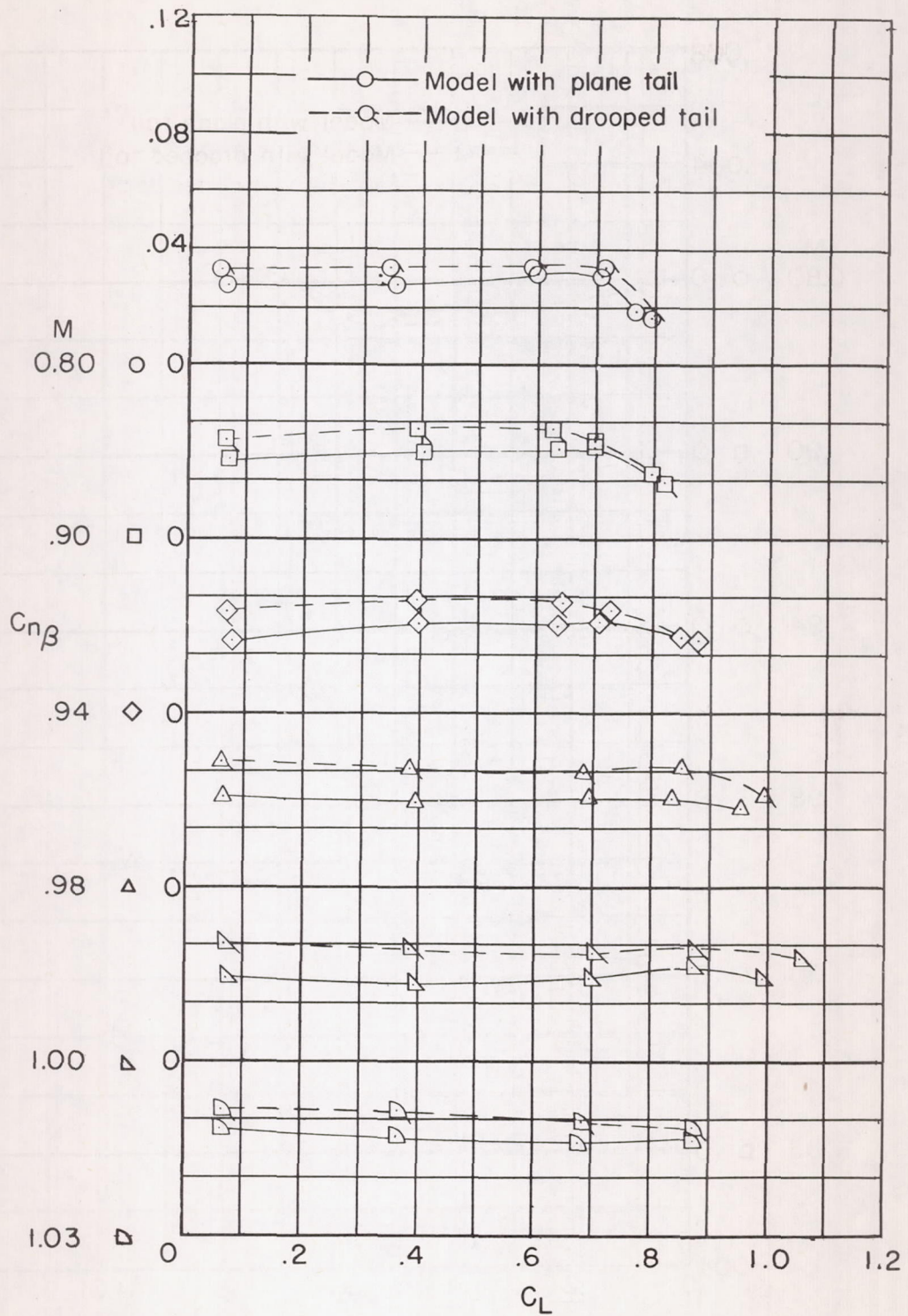
(b) $C_{n\beta}$ against C_L .

Figure 12.- Continued.

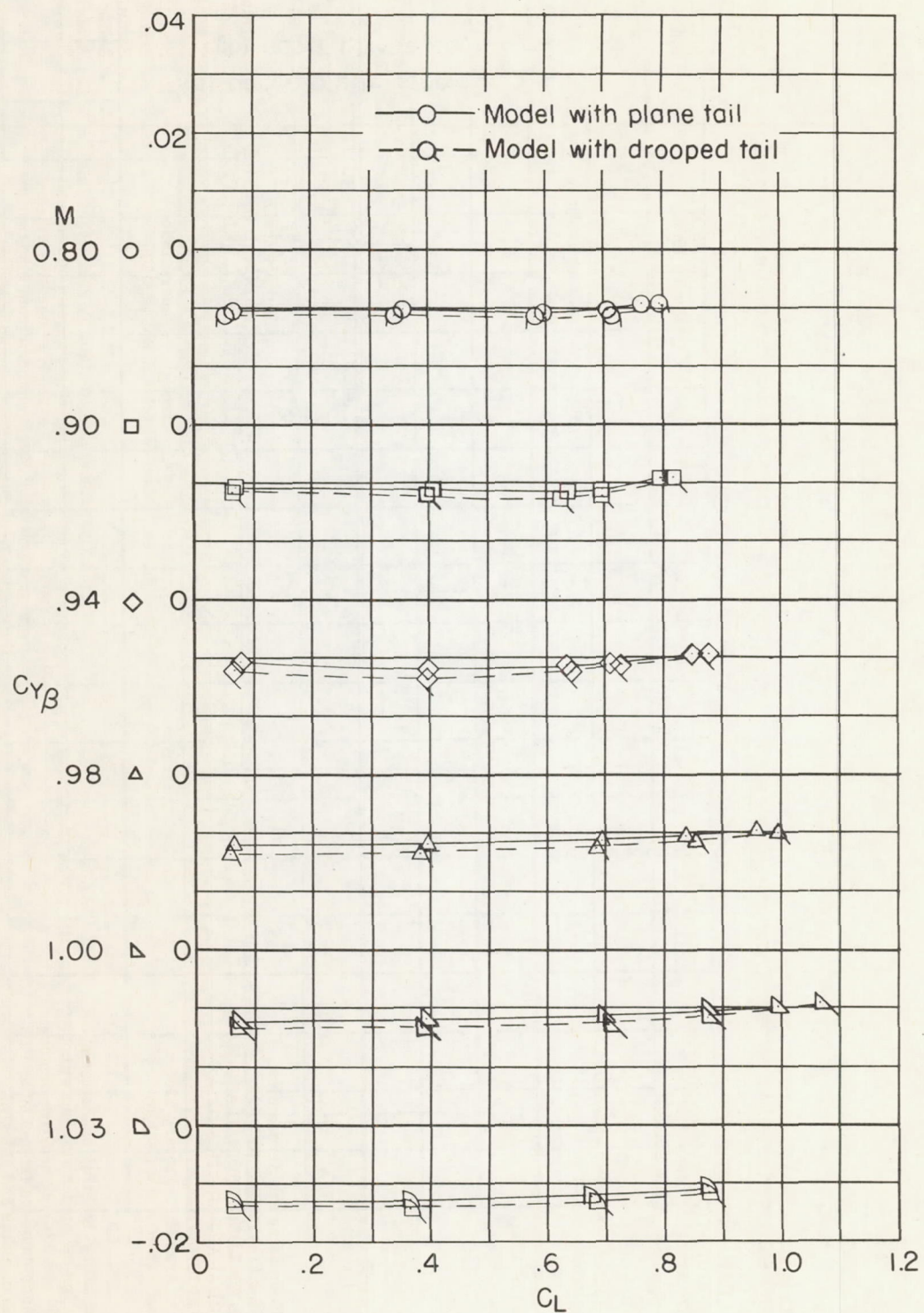
(c) $C_{Y\beta}$ against C_L .

Figure 12.- Concluded.